Journal of Medicinal Chemistry

pubs.acs.org/jmc Article

Rational Design of Photochromic Analogues of Tricyclic Drugs

Fabio Riefolo, Rosalba Sortino,[¶] Carlo Matera,[¶] Enrique Claro, Beatrice Preda, Simone Vitiello, Sara Traserra, Marcel Jiménez, and Pau Gorostiza*

Cite This: *J. Med. Chem.* 2021, 64, 9259−9270 Read Online

ACCESS | Metrics & More | Article Recommendations | Supporting Information

ABSTRACT: Tricyclic chemical structures are the core of many important drugs targeting all neurotransmitter pathways. These medicines enable effective therapies to treat from peptic ulcer disease to psychiatric disorders. However, when administered systemically, they cause serious adverse effects that limit their use. To obtain localized and on-demand pharmacological action using light, we have designed photoisomerizable ligands based on azobenzene that mimic the tricyclic chemical structure and display reversibly controlled activity. Pseudo-analogues of the tricyclic antagonist pirenzepine demonstrate that this is an effective strategy in muscarinic acetylcholine receptors, showing stronger inhibition upon illumination both *in vitro* and in cardiac atria *ex vivo*. Despite the applied chemical modifications to make pirenzepine derivatives sensitive to light stimuli, the most potent candidate of the set, cryptozepine-**2**, maintained a moderate but promising M_1 vs M_2 subtype selectivity. These photoswitchable "crypto-azologs" of tricyclic drugs might open a general way to spatiotemporally target their therapeutic action while reducing their systemic toxicity and adverse effects.

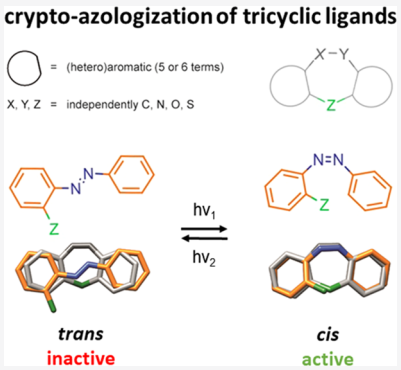

INTRODUCTION

Photopharmacology is a modern branch of pharmacology that aims to improve the efficacy and safety of drugs by directing their action to target organs and controlling their doses using light. It deals with molecular strategies to photoregulate drug activity.[1,2] Most photoswitchable small molecule ligands developed in recent years have exploited the reduced size and robust photochromism of azobenzene, which allows two design approaches: (1) tailoring compounds through the extension of the drug core ("azo-extension" approach) and (2) introducing an isosteric azobenzene photoswitch in the core ("azologization" approach).[3,4] The latter is the most straightforward design strategy and is generally preferred because it requires minimal modifications of the original structure, thus maintaining the drug-likeness of the parent compound and largely preserving its pharmacokinetic and pharmacodynamic properties.[5,6] If azologization motifs are not present, in some cases, the drug structure can be extended with a photoswitchable moiety while retaining the drug activity.[3,7] However, these versatile and complementary strategies are not applicable to all drugs. This is often the case when azobenzene-like motifs are absent from a parent molecule that can only tolerate minor variations in size (i.e., nonazologizable and nonazo-extendable drugs), thus hampering the reach of photopharmacology. An important class of drugs that have not been endowed with photoregulation is characterized by the general formula, shown in Figure 1A, i.e., those fused tricyclic compounds, which are known as "privileged structures" in medicinal chemistry.[8] This term was coined by Ben Evans in 1988 to recognize the potential of certain structural motifs as templates for the derivatization and discovery of novel biological ligands.[9] A great diversity of tricyclic derivatives has been developed and are marketed for different clinical conditions. They include central nervous system agents such as tricyclic antidepressants used to treat psychiatric disorders[10] but also for other therapeutic indications such as loratadine (an antihistamine drug used to treat the symptoms of allergies), nevirapine (a noncompetitive HIV-1 reverse transcriptase inhibitor), lonafarnib (a farnesyl transferase inhibitor used as anticancer), and pirenzepine (PNZ) (an antimuscarinic drug to treat peptic ulcers).[11]

An arylazo moiety (e.g., an azobenzene) in its *cis* configuration can quite resemble (at least in some of its conformations) the geometry of the tricyclic scaffold, whereas the corresponding *trans* isomer cannot. This is illustrated by the three-dimensional alignment of conformers in Figure 1B. Thus, we devised a way to mimic the tricyclic system of these drugs with a photochromic arylazo unit by means of two modifications: (1) the isosteric substitution of the two-atom bridge connecting the aryl rings with a −N═N− group to confer photochromic behavior and (2) the cleavage (ring opening) of one of the two single bonds forming the one-atom bridge to increase the flexibility and to enable greater changes

Received: March 19, 2021
Published: June 23, 2021

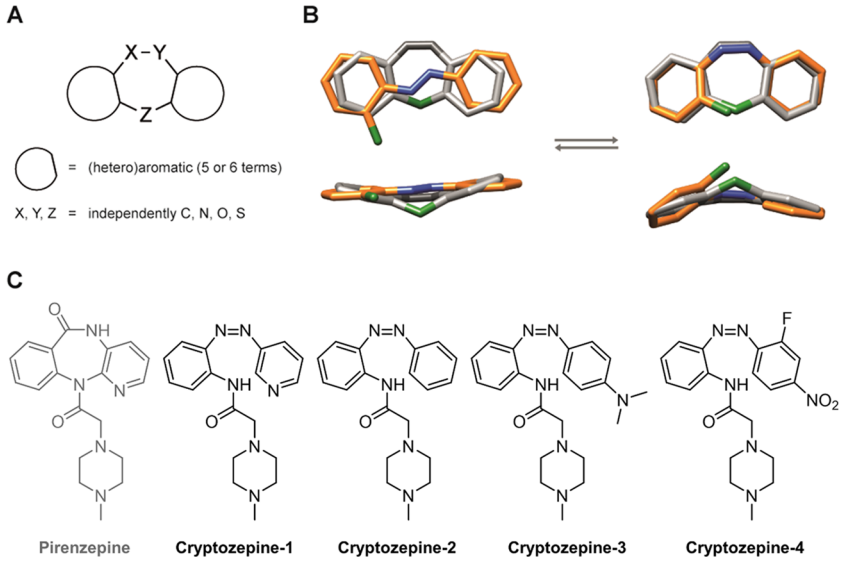

Figure 1. Design strategy and structure of crypto-azologs. (A) General scaffold of fused tricyclic drugs. (B) Best three-dimensional alignment of an azobenzene scaffold (*trans* on the left and *cis* on the right, both in orange) over a generic fused tricyclic system (in gray). For the sake of comparison, the carbon atom of the 1-atom bridge of the tricyclic system and the corresponding carbon atom of the azobenzene are indicated in green. Nitrogen atoms are in blue. (C) Chemical structure of the muscarinic M_1 antagonist pirenzepine and the cryptozepines, the photochromic derivatives discussed in this work.

in geometry upon photoisomerization. In this way, the photochromic pseudo-analogue of the tricyclic drug should be able to maintain the pharmacological properties of the parent compound upon photoisomerization to the *cis* configuration. Conversely, the most thermodynamically stable *trans* isomer should display a reduced capacity to modulate its biological target. This situation would be particularly favorable to apply the inactive drug in the absence of illumination and to photoactivate it at the desired locations and times. We named this novel procedure to design photoswitchable small molecules "crypto-azologization" (where the prefix "crypto-" comes from the Ancient Greek word *κρυπτός* [kruptós], meaning "hidden") because it expands the azologization strategy to compounds in which the potential photochromic scaffold is buried and must be sculpted out of the parent structure by a ring opening in addition to the canonical azosteric replacement.

As a test bed for our design strategy, we chose the muscarinic acetylcholine receptor (mAChR) antagonist pirenzepine (Figure 1C), both because of its tricyclic structure and therapeutic importance. Muscarinic receptors belong to the class A family of G-protein-coupled receptors (GPCRs) and are classified into five distinct subtypes.[12,13] The wide distribution of mAChRs in the body and the limited subtype selectivity of muscarinic drugs are the cause of their adverse effects, which have made these receptors an attractive target in photopharmacology.[14−16] Pirenzepine (Gastrozepine) is an M_1-selective muscarinic antagonist marketed to treat peptic ulcers. In particular, it inhibits the parasympathetic nervous system "rest-and-digest" response, reducing gastric acid secretion and muscle spasm.[17−20] Other potential applications have been considered, like slowing down myopia progression[21] and reducing the risk of lethal events in the ischemic heart disease.[22] The wide expression of M_1 mAChRs in the hippocampus and medial prefrontal cortex suggests that M_1-mediated signaling is important for cognitive and learning functions and plays a key role in several neurological disorders.[12,13] The development of photoswitchable M_1 ligands is thus of great interest for both therapeutic and research purposes. Here, we report the synthesis of photoswitchable M_1 mAChR antagonists designed by crypto-azologization of pirenzepine and the characterization of their photopharmacological effects *in vitro* and *ex vivo*.

RESULTS AND DISCUSSION

Rational Design and Chemical Synthesis. As an initial control for our design strategy, we performed docking simulations of a representative structure at the M_1 mAChR.[23] The results supported our hypothesis (see the SI for details) and encouraged us to pursue the synthesis of a small set of pirenzepine crypto-azologs that were named "cryptozepines" (Figure 1C). Previous studies on pirenzepine congeners have shown how the nature and placement of accessory groups on the central core of the molecule determine the differences in receptor recognition and the binding process at mAChRs.[19] In particular, the positioning of the protonated nitrogen atom at the end of the piperazine, which is affected by the geometry of the whole structure, is crucial for the receptor recognition and the binding processes in M_1 mAChRs.[19,23,24] On the other hand, certain structural modifications at the tricyclic core are tolerated. The endocyclic amide group is thought to participate in polar interactions at the binding site; therefore, its replacement with a lipophilic function such as an ethylene bridge would likely produce a loss of affinity, whereas an azo group could be better accepted. The exocyclic amide group and the nitrogen atom in one of the two aromatic rings seem to have only a minor effect in terms of affinity and selectivity.[19] As such, we decided to conserve the essential 2-(4-methylpiperazin-1-yl)acetamide side chain in all of the novel derivatives, while the endocyclic amide group was replaced with an azo group and the central seven-membered ring was "opened" to generate a fully unconstrained photochromic unit. In addition, structural variations at this unit were rationally designed to obtain analogues endowed with different photochemical properties. Cryptozepine-**1** and cryptozepine-**2**

https://doi.org/10.1021/acs.jmedchem.1c00504
J. Med. Chem. 2021, 64, 9259−9270

Scheme 1. Chemical Synthesis of Cryptozepines

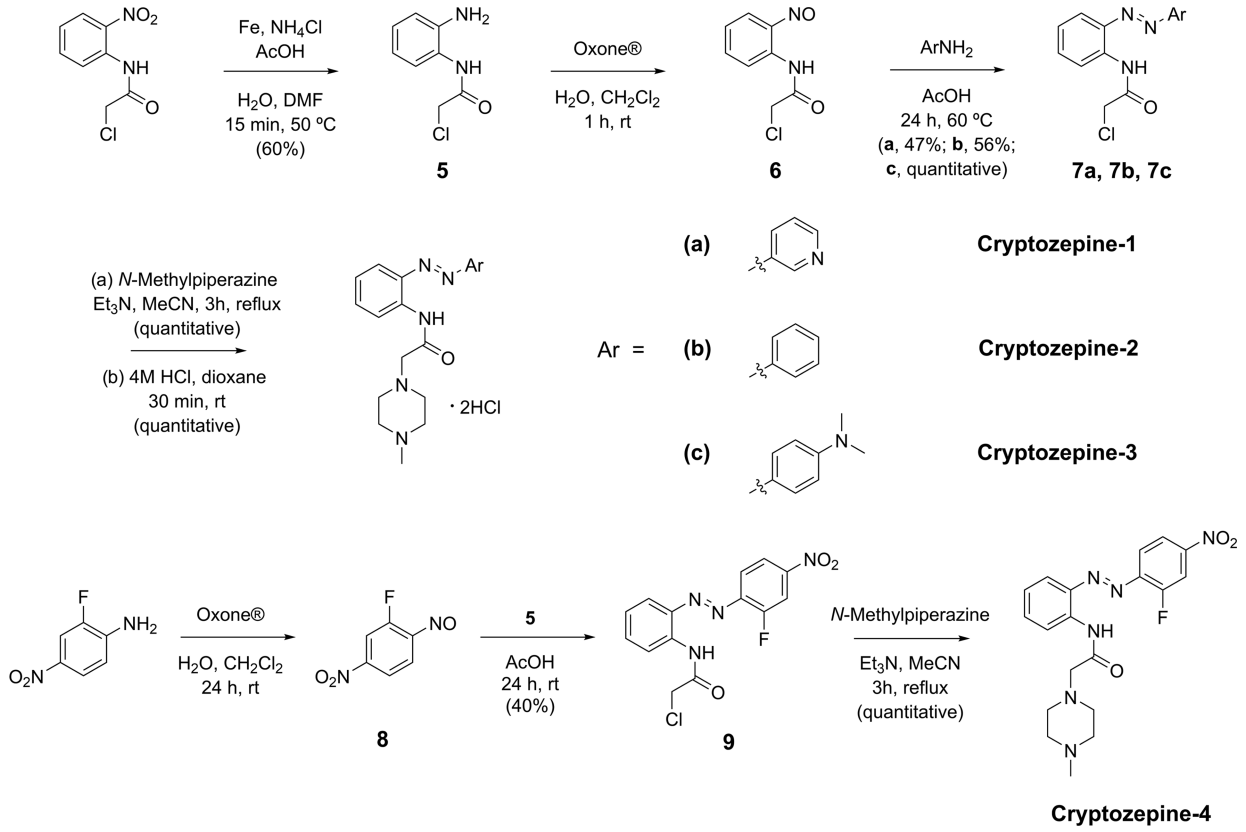

are straightforward crypto-azologs of pirenzepine and differ from one another in the presence of the nitrogen atom in one of the two aromatic rings of criptozepine-**1**. This feature should significantly reduce the half-life of thermal relaxation of the *cis* isomer, as well as increase the aqueous solubility of this derivative. We expected, though, that these two derivatives would need ultraviolet (UV) light to undergo *trans*-to-*cis* isomerization, which is generally not convenient in biology.[25] Cryptozepine-**3** was designed to overcome this limitation by introducing an electron-donating group ($-NMe_2$) at the *para* position of the benzene ring, which is not directly connected to the side chain, to produce a red-shifting "push−pull" effect (Figure 1C).[26] A fourth compound, cryptozepine-**4**, characterized by a different "push−pull" system, was designed and prepared, but because of its very low aqueous solubility at neutral pH, we could not test its pharmacological properties. However, its physicochemical characterization is reported in the SI.

As mentioned above, we hypothesized that the M_1 mAChR should be able to properly accommodate the new ligands in their *cis* configuration, while the *trans* geometry should hinder the rest of the molecule from entering the binding pocket. Cryptozepines **1**, **2**, and **3** were synthesized as illustrated in Scheme 1. *N*-Chloroacetyl-2-nitroaniline was reduced to the corresponding amine (**5**) by treating with iron in ammonium chloride and acetic acid. Oxidation with Oxone gave the nitroso derivative (**6**), which was then coupled to the chosen arylamine under Mills conditions to yield the arylazo intermediates (**7a**, **7b**, **7c**). Nucleophilic substitution of chlorine with 1-methylpiperazine and subsequent treatment with hydrochloric acid afforded the three final compounds as dihydrochloride salts (**1**, **2**, and **3**). To synthesize cryptozepine-**4** (Scheme 1), 2-fluoro-4-nitroaniline was oxidized with Oxone to give the nitroso derivative (**8**), which was then coupled to the corresponding amine (**5**) under Mills conditions to yield the arylazo intermediate (**9**). Nucleophilic substitution of chlorine with 1-methylpiperazine afforded cryptozepine-**4**.

Photochemical Characterization. We then tested the ability of our photoswitchable compounds to respond effectively to light. First, we characterized the three cryptozepines by UV−vis spectroscopy. Cryptozepines **1** and **2** displayed a clear photochromic behavior and the typical absorption bands of azobenzenes in water, with maxima at 318 and 433 nm due to $\pi-\pi^*$ and $n-\pi^*$ transitions, respectively (Figure 2 and SI). As expected, the presence of an electron-donating group in cryptozepine-**3** resulted in a strong red-shift of the $\pi-\pi^*$ transition band, with an absorption maximum at 465 nm in an aqueous solution. In this case, it was not possible to observe any change in the absorption spectrum with steady-state spectroscopy in an aqueous solution since the thermal isomerization of this kind of azobenzenes in protic solvents occurs extremely fast and generally completes within milliseconds.[27] However, we proved the capacity of compound **3** to photoisomerize in a dry organic solvent (Figure 2 and SI). We then determined the photostationary distribution of cryptozepines **1** and **2** by ^1H NMR analysis. The distribution changed from about 90% in favor of the *trans* form in the dark to about 10% (90% in favor of the *cis* form) after illumination with UV light (365 nm) for both compounds. Compounds **1** and **2** also showed a good thermal stability, with a half-life of thermal relaxation of 71 and 182 min, respectively (Figure 2 and SI).

Competition Binding and Calcium Imaging Experiments at Muscarinic Receptors. We determined the affinity

https://doi.org/10.1021/acs.jmedchem.1c00504
J. Med. Chem. 2021, 64, 9259−9270

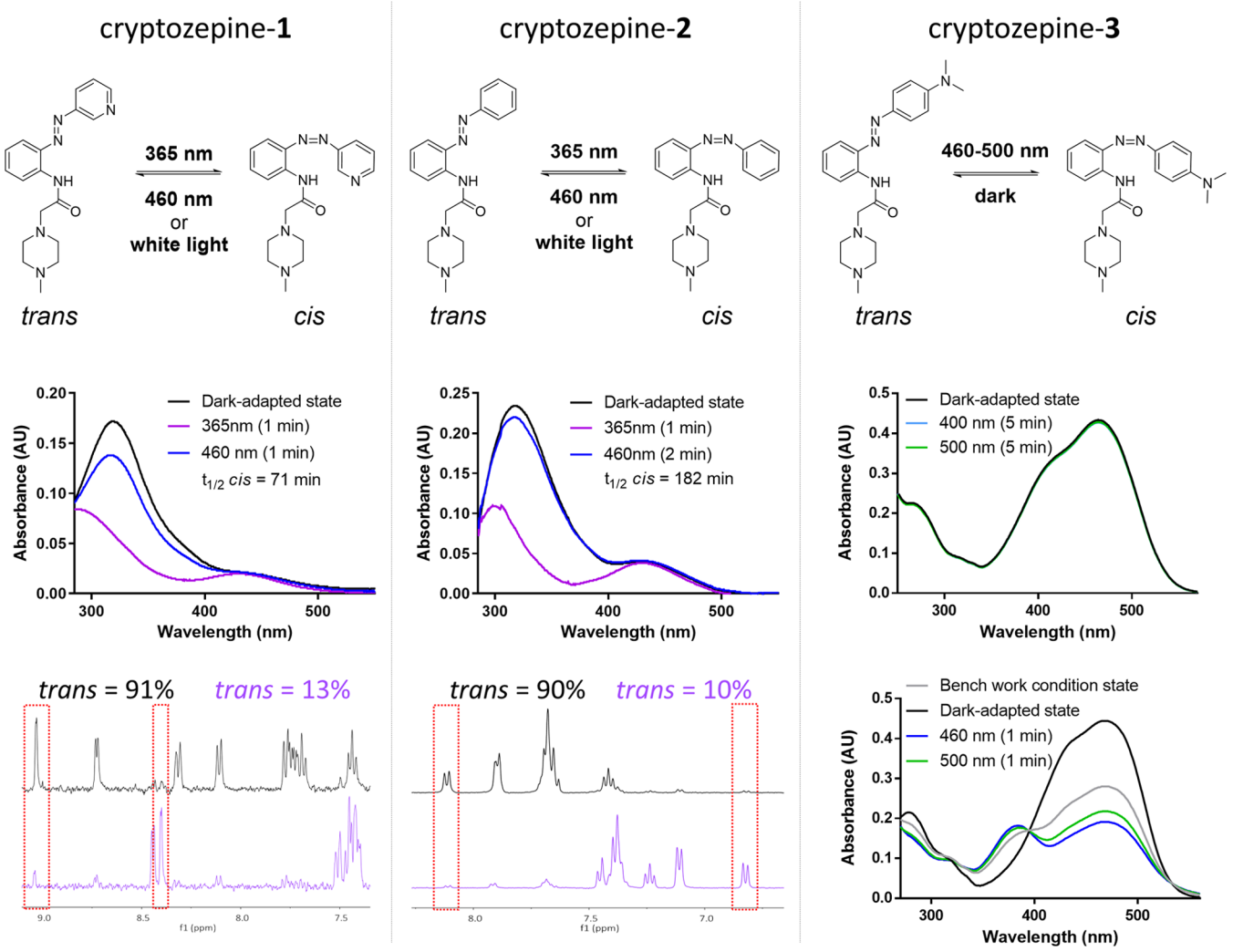

Figure 2. Photochemical characterization. Left column: absorption spectra (30 μM in H_2O) and quantification of the cryptozepine-**1** photostationary state (PSS) by ^1H NMR analysis (1 mM in D_2O), showing the ratio between the two isomers in the dark-adapted state (*trans* = 91%) and after illumination with 365 nm light for 5 min (*trans* = 13%). Middle column: absorption spectra (30 μM in H_2O) and quantification of cryptozepine-**2** PSS by ^1H NMR analysis (1 mM in D_2O), showing the ratio between the two isomers in the dark-adapted state (*trans* = 90%) and after illumination with 365 nm light for 5 min (*trans* = 10%). Right column: absorption spectra in water (30 μM, spectra above) and absorption spectra in anhydrous dimethyl sulfoxide (DMSO) (30 μM, spectra below) of cryptozepine-**3**. The switching of the red-shifted compound cryptozepine-**3** can be observed by UV−vis spectrophotometer analysis only in an anhydrous solvent.

of pirenzepine and cryptozepines for the mAChRs by radioligand competition binding assays. For this purpose, we used Wistar rat brain membranes (whole cortex), which contain a high density of mAChRs,[28] and the nonselective muscarinic orthosteric antagonist [^3H]quinuclidinyl benzilate ([^3H]QNB) as a competitive radioligand (see the SI).[28−31] In this assay, pirenzepine has a good binding affinity in the nanomolar range, with an IC_{50} of about 50 nM (Table 1, and SI, Figure S5.1), and all cryptozepines showed a moderate binding affinity in the low micromolar range, with cryptozepine-**2** emerging as the best ligand with an IC_{50} of about 9 μM (Table 1, and SI, Figure S5.1). No significant differences in affinity were observed between the *trans*- and the *cis*-enriched forms (named "*trans*" and "*cis*" hereafter for the sake of simplicity) for the three cryptozepines in these experimental conditions. However, the fact that the compounds maintain the muscarinic binding despite the cleavage of the original tricyclic core encouraged us to further investigate their photopharmacological behavior through activity assays where differences between the *trans* and *cis* forms might be detected.

Table 1. Muscarinic Radioligand Competition Binding Assays in Wistar Rat Brain Membranes[a]

ligand	K_i (M)	IC_{50} (M)
pirenzepine	8.4 (±1.4) × 10^{-9}	5.0 × 10^{-8}
cryptozepine-**1** (*trans*)	6.4 (±1.4) × 10^{-6}	3.8 × 10^{-5}
cryptozepine-**1** (*cis*)	7.0 (±2.2) × 10^{-6}	4.2 × 10^{-5}
cryptozepine-**2** (*trans*)	1.7 (±0.3) × 10^{-6}	9.9 × 10^{-6}
cryptozepine-**2** (*cis*)	1.5 (±0.5) × 10^{-6}	9.2 × 10^{-6}
cryptozepine-**3** (*trans*)	5.3 (±0.1) × 10^{-6}	3.3 × 10^{-5}
cryptozepine-**3** (*cis*)	5.3 (±0.1) × 10^{-6}	3.2 × 10^{-5}

[a]The parameters shown in the table were calculated using the "Binding−Competitive−one site−Fit Ki" for K_i values and "Binding−Competitive−one site−Fit logIC50" for the IC_{50}, which are functions in GraphPad Prism 6. Values are mean ± SEM.

In particular, our data suggested retaining cryptozepine-**2** (best binding affinity) and cryptozepine-**3** (best photochromic

https://doi.org/10.1021/acs.jmedchem.1c00504
J. Med. Chem. 2021, 64, 9259−9270

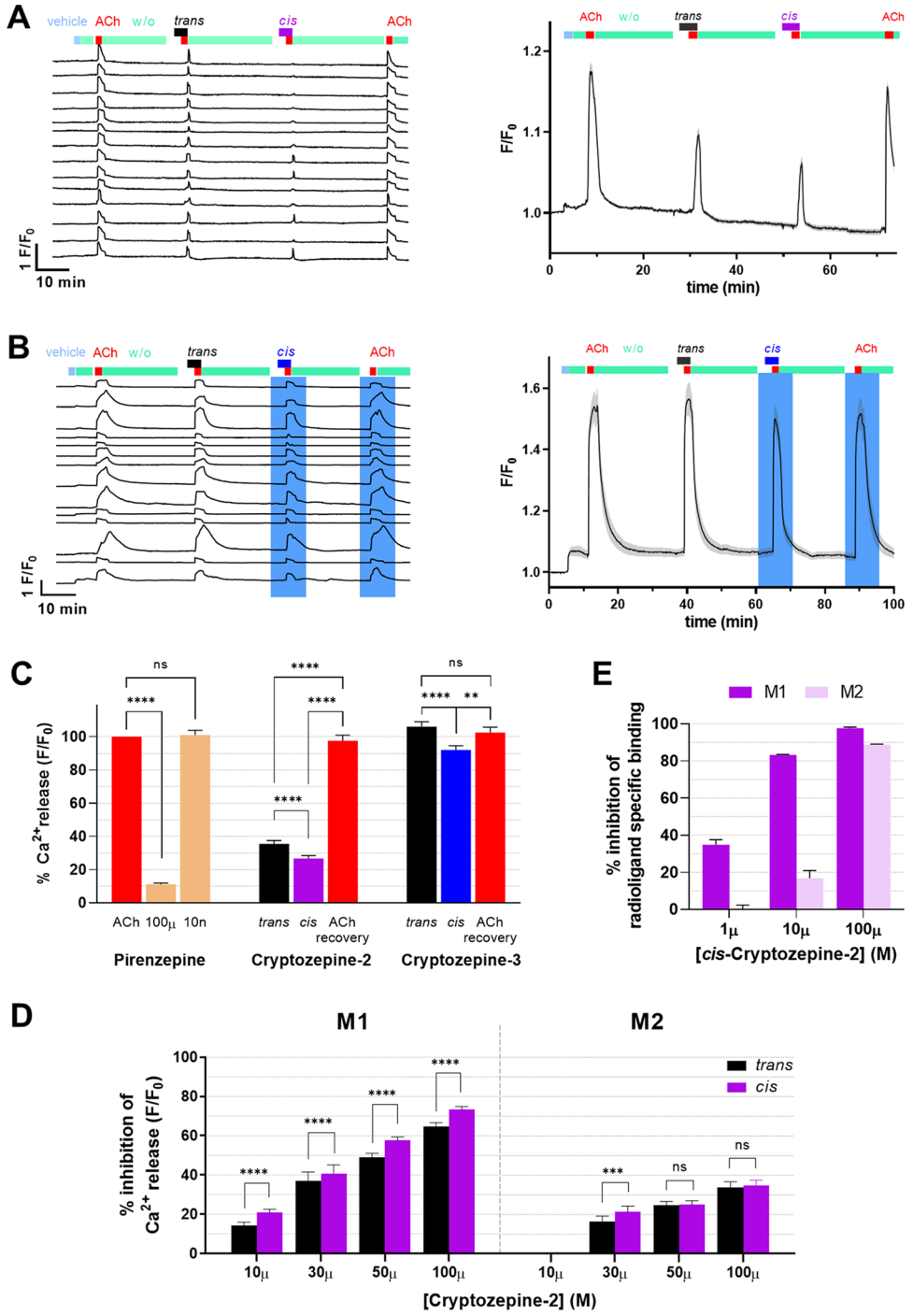

Figure 3. Cryptozepine-**2** and -**3** antagonism on M_1 mAChRs and cryptozepine-**2** subtype selectivity. (A) Cryptozepine-**2** and (B) cryptozepine-**3** real-time calcium imaging response from HEK cells expressing M_1 mAChRs, loaded with 10 μM calcium indicator OGB-1 AM (representative single traces, n = 14 cells, on the left; average, n = 67 cells, on the right), and coexpressing R-GECO1 as a calcium indicator (representative single traces, n = 14 cells, on the left; average, n = 48 cells, on the right), respectively. After 365 nm illumination, 100 μM cryptozepine-**2** reduced 0.5 μM ACh responses stronger than before UV light application. Under 460 nm illumination, 100 μM cryptozepine-**3** reduced 0.5 μM ACh responses. The gray band indicates the standard error of the mean (SEM). (C) Quantification of the calcium imaging responses. ACh-induced calcium release was significantly reduced by 100 μM pirenzepine and cryptozepine-**2**. *cis*-Cryptozepine-**2** shows a significantly stronger inhibition than its *trans* isomer. Cryptozepine-**3** (100 μM) partially and significantly reduced ACh-induced calcium release only under 460 nm illumination (*cis*). Data were analyzed by paired-sample Wilcoxon signed-rank test (p-value (**) < 0.01, (***) < 0.001, (****) < 0.0001; GraphPad Prism 6). Error bars are ± SEM. (D) Calcium imaging studies of M_1 vs M_2-GqTOP selectivity with 10 (M_1, n = 183; M_2, n = 99), 30 (M_1, n = 58; M_2, n = 106), 50 (M_1, n = 262; M_2, n = 191), and 100 (M_1, n = 194; M_2, n = 165) μM cryptozepine-**2**. On M_1-expressing cells, cryptozepine-**2** significantly showed its stronger and photoswitchable antagonism than on M_2 cells. The data were normalized over the maximum response obtained with 0.5 μM ACh and analyzed by the paired-sample Wilcoxon signed-rank test (p-value (***) < 0.001, (****) < 0.0001; GraphPad Prism 6). Error bars are ± SEM. (E) Selective M_1 vs M_2 mAChR radioligand binding inhibition of the more active *cis*-cryptozepine-**2** isomers.

https://doi.org/10.1021/acs.jmedchem.1c00504
J. Med. Chem. 2021, 64, 9259−9270

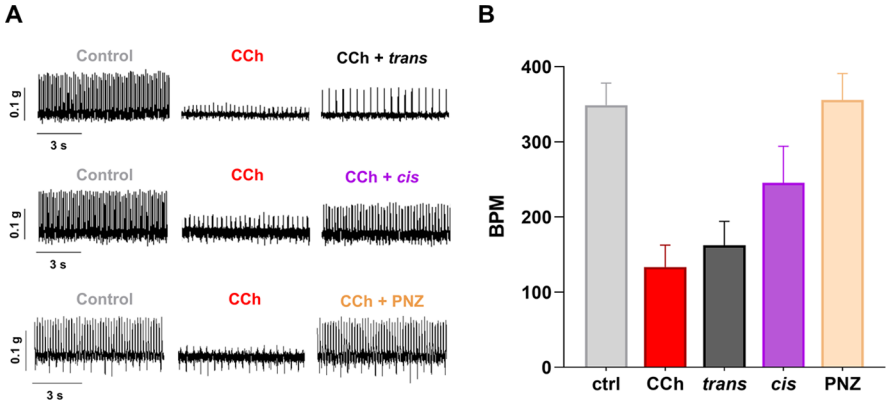

Figure 4. Pirenzepine and cryptozepine-**2** can antagonize CCh-induced bradycardia in mouse atria through M_1 receptors. Representative traces (A) and quantification (B) of mouse right atrium heart rate treated with carbachol (CCh), pirenzepine (PNZ), and *trans*/*cis*-cryptozepine-**2**. Spontaneous mechanical contractions of the mouse atria were recorded as control (ctrl) and defined as the heartbeat frequency in beats/min (BPM). CCh (1 μM) decreased both the amplitude and BPM. The presence of PNZ ($n = 6$) and *cis*-cyptozepine-**2** (*cis*) ($n = 2$) reversed the CCh-induced bradycardia. In contrast, *trans*-cryptozepine-**2** (*trans*) ($n = 2$) did not reverse the effect of CCh in terms of the heartbeat frequency ($n = 2$).

behavior) for further studies. We performed real-time calcium imaging experiments in transiently transfected HEK cells expressing M_1 mAChR to study the antagonist behavior of our compounds (Figure 3). The calcium indicator OGB-1 AM (excitation at 494 nm and emission at 523 nm) was suitable for cryptozepine-**2**, while R-GECO1 (excitation at 561 nm and emission at 589 nm) was used for cryptozepine-**3** to avoid artifacts due to unwanted emission of fluorescence from OGB-1 AM upon illumination at 460 nm. The natural orthosteric agonist acetylcholine (ACh, 0.5 μM) was applied or coapplied to induce receptor activation. ACh alone induced reproducible cytosolic calcium oscillations, indicative of M_1 agonism. Both cryptozepines-**2** and **3** at 100 μM showed antagonistic behavior. Importantly, a complete recovery of ACh-induced activity was observed after the complete wash-out of the two antagonists. At 100 μM, cryptozepine-**2** reduced the total cell response by 64% (mean) (±2.1; standard error of the mean [SEM]) in *trans* and by 73% (±1.6) in *cis*. Cryptozepine-**3** did not antagonize the ACh-induced response at 100 μM in *trans*, and it reduced the cell response by 14% (±2.6) under continuous illumination (*cis*-enriched form) with blue light (460 nm) (Figure 3). The antagonist activity and the significant differences observed between the *trans* and *cis* states for both compounds are in agreement with the design, where a higher inhibitory activity was intended upon illumination. The stronger inhibition displayed by cryptozepine-**2** compared to cryptozepine-**3** at 100 μM is probably due to the three-fold tighter binding of the former (see the SI, Figure S5.1). The activity of *trans*-cryptozepine-**2** can also be attributed to its proximity to saturation at this concentration and could be reduced at lower concentrations. Correspondingly, cryptozepine-**3** is inactive in the dark and a (weak) inhibitor under illumination with blue light at the same concentration. We hypothesized that the electronic and/or steric properties of the additional group ($-NMe_2$) on the terminal aromatic ring in cryptozepine-**3** might account for its reduction of efficacy in comparison with cryptozepine-**2**. However, the efficiency of cryptozepine-**3** may also be limited by the relatively smaller population of the *cis* isomer that is achieved upon irradiation as a consequence of its faster relaxation. Before using our most potent antagonist, cryptozepine-**2**, for physiologically more complex experiments, we studied whether it also retained the M_1 vs M_2 subtype selectivity of pirenzepine. First, we measured calcium responses in HEK cells expressing M_2 mAChR and observed that the antagonist behavior of cryptozepine-**2** was only partial (100 μM) or undetectable (10 μM) for this receptor subtype (Figure 3D). We also tested the M_1/M_2 specific affinity of the more active *cis*-cryptozepine-**2** in radioligand competition binding studies. These results also confirmed the M_1 selectivity in the μM range of concentrations (1, 10, and 100 μM), with a quite negligible M_2 affinity at 1 and 10 μM (Figure 3E) and estimated IC_{50} values of 1.9 μM for M_1 and 28 μM for M_2 (Figure S5.2). These data altogether demonstrate that the crypto-azologization design yields *cis*-active light-sensitive derivatives that retain not only the original activity of the parent compound but also its selectivity.

Anticholinergic Effects in Mouse Isolated Atrium. To validate crypto-azologs in a physiologically relevant scenario (i.e., in tissue expressing a diversity of endogenous receptors), we tested the effect of cryptozepine-**2** on the mouse isolated atrium. Here, the excitation of muscarinic receptors induces arrest of the heartbeat.[32−34] This negative chronotropic effect in the atria is primarily mediated by mAChR activation, including M_1, and the anticholinergic activity of pirenzepine resumes the heart rate and rhythm.[32−35] We isolated the right atria from male mice and measured their spontaneous frequency of contraction (control), which was about 360 beats/min (see the SI). Application of the muscarinic agonist carbachol (CCh, 1 μM) strongly reduces the frequency to around 200 beats/min (Figure 4), and the addition of pirenzepine (PNZ, 1 μM) to the bath restores the frequency almost to control values (Figure 4). We used this robust assay to test the antagonist behavior of cryptozepine-**2** isomers. At a concentration of 100 μM, the *trans* isomer was unable to antagonize CCh-induced bradycardia and was seemingly inert, whereas *cis*-cryptozepine-**2** readily induced the partial recovery of the atrium contraction frequency (Figure 4 and SI). This effect is in accord with the M_1 anticholinergic activity of pirenzepine in the atria[32−35] and, considering the partial M_1 vs M_2 selectivity of our ligand at 100 μM (Figure 3), can be attributed mainly to M_1, further highlighting the pharmacological potential of the crypto-azologization design.

Regarding future applications, the photopharmacological properties of cryptozepines should be enhanced by improving the potency of the active forms and avoiding the need for

https://doi.org/10.1021/acs.jmedchem.1c00504
J. Med. Chem. 2021, 64, 9259−9270

ultraviolet light, which is not optimal for biological applications. Although it is remarkable that crypto-azologs retain the activity and selectivity of the parent tricyclic compound, the actual potency achieved in our pilot study is almost 200-fold lower (see Table 1), which prompts subsequent rounds of lead optimization and safety testing as usually carried out in drug development processes. An option for improving the optical and pharmacological properties at once might be inserting fluorine in the ortho position(s) of the azobenzene. These modifications should preserve or even improve the antagonist potency by adding lipophilic contacts in the binding pocket[16] while providing favorable photochromic properties like slow thermal back-isomerization and high two-photon cross-section.[36] Furthermore, substitutions of the piperazine tail allow tuning subtype selectivity, e.g., diethyl[(piperidin-2-yl)methyl]amine yields nanomolar, M_2 selective antagonists.[37,38]

Overall, the photopharmacological properties of cryptozepines set the stage for interesting assays *in vivo*. If they can be enterically administered in the inactive form (*trans*), these drugs could be remotely photoactivated at the desired location and time using the built-in light-emitting diode (LED) of an endoscopy capsule,[39] potentially allowing to treat gastrointestinal tract diseases without producing (adverse) effects in other regions or organs. More invasive applications include the manipulation of cardiac function *in vivo* using optoelectronic devices coupled to cardiac patches.[14,40] In any case, to test the feasibility of future therapies based on photoswitchable drugs, both isomers must be pharmacologically characterized.

CONCLUSIONS

In summary, we have expanded the rational design of photochromic ligands to the important class of tricyclic drugs. The proposed strategy involves two concomitant structural modifications to afford azobenzene derivatives that can mimic the tricyclic motif: (1) an isosteric replacement with a −N═N− group and (2) a ring cleavage. We have demonstrated a proof of concept with a set of photoswitchable derivatives of the muscarinic antagonist pirenzepine that we named cryptozepines. These novel compounds retain micromolar binding and antagonist character despite the structural dissimilarity with the parent compound. The most potent photoswitchable compound (cryptozepine-**2**) displays negligible activity in mouse atrium in *trans* and M_1 antagonism in *cis*, indicating that the crypto-azologization strategy has the potential to produce photoswitchable derivatives of tricyclic drugs that are inactive in their thermally stable *trans* isomer, which is desirable in photopharmacology. Further optimization of photochromism and the potency of the active form might yield photopharmacological drug candidates, displaying high safety and localized therapeutic action. Interestingly, cryptozepine-**2** already maintains a moderate selectivity for M_1 over M_2 receptors, similar to its parent compound. The proof of concept demonstrated with this strategy opens the way to use it in many other targets bearing the tricyclic motif. This work provides a new toolbox to design photochromic drugs that significantly expands the scope of photopharmacology and its applications.

EXPERIMENTAL SECTION

Chemical Synthesis. *Materials and Methods.* All reagents and solvents were purchased from Sigma-Aldrich, Cymit Química, and Serviquimia and were used without any further purification. Thin-layer chromatography (TLC) analyses were performed on commercial silica gel 60 F_{254} aluminum foils (Merck); spots were further evidenced by spraying with a dilute alkaline potassium permanganate solution or a 5% phosphomolybdic acid solution in ethanol and, for tertiary amines and quaternary ammonium compounds, with the Dragendorff reagent. Flash chromatography was performed on PanReac AppliChem silica gel 60 (40−63 μm), Biotage SNAP KP-C18-HS 12 g or Biotage SNAP KP-SIL 25 g as stationary phases; mobile phases are specified for each compound. UV−vis spectra and experiments were recorded with a Shimadzu UV-1800 UV−Vis Spectrophotometer with standard quartz cuvettes (10 mm light path). ^{1}H NMR and ^{13}C NMR spectra were registered with a Varian Mercury 400 MHz (400 MHz for ^{1}H NMR and 101 MHz for ^{13}C NMR) and a Varian VNMRS 500 MHz instrument (500 MHz for ^{1}H NMR and 126 MHz for ^{13}C NMR) in DMSO-d_6, $CDCl_3$, and D_2O. Residual signals of the deuterated solvents were used as an internal standard (DMSO-d_6: ^{1}H 2.50 ppm, ^{13}C 39.52 ppm; $CDCl_3$: ^{1}H 7.26 ppm, ^{13}C 77.16 ppm; D_2O: ^{1}H 4.79 ppm). Chemical shifts (δ) are expressed as parts-per-million (ppm) and coupling constants (J) as hertz (Hz). High-performance liquid chromatography (HPLC) analyses were performed with a Waters Alliance 2795 separation module (RP column: XSelect CSH C18, 50 × 4.6 mm^2, S-3.5 μm, 1.6 mL/min; eluent: from 5% B to 100% B in 3.5 min using a linear gradient, A: H_2O 0.1% formic acid, B: acetonitrile 0.1% formic acid) coupled to a Waters 2996 photodiode detector and a Waters 3100 mass spectrometer. High-resolution mass spectroscopy measurements (ionization: NanoESI, positive ionization) were performed at the mass spectrometry core facility of the IRB (Barcelona, Spain) with an LTQ-FT Ultra (Thermo Scientific) for direct infusion (Automated Nanoelectrospray) of the sample. The NanoMate (Advion BioSciences, Ithaca, NY) aspirated the samples from a 384-well plate (protein LoBind) with disposable, conductive pipette tips and infused the samples through the NanoESI Chip (which consists of 400 nozzles in a 20 × 20 array) toward the mass spectrometer. Spray voltage was 1.70 kV and delivery pressure was 0.50 psi. Data are reported as a mass-to-charge ratio (m/z) of the corresponding positively charged molecular ions.

Abbreviations. Solvents: EtOAc, ethyl acetate; CH_2Cl_2, dichloromethane; MeCN, acetonitrile; MeOH, methanol; EtOH, ethanol; THF, tetrahydrofuran; Et_2O, diethyl ether; DMSO, dimethyl sulfoxide. Analytical characterization: NMR: d, doublet; dd, double doublet; ddd, double double doublet; dddd, doublet of doublet of doublet of doublets; dt, double triplet; m, multiplet; q, quartet; quin, quintet; s, singlet; t, triplet; m.p., melting point; R_f, retention factor; r.t., room temperature; RT, retention time.

Detailed characterization data are disclosed in the Supporting Information (SI).

*N-(2-Aminophenyl)-2-chloroacetamide (**5**).* Fe (1.30 g, 23.30 mmol), NH_4Cl (124.63 mg, 2.33 mmol), and glacial acetic acid (0.270 mL, 4.66 mmol) were added into 10 mL of H_2O and stirred at 50 °C for 15 min. A solution of 2-chloro-*N*-(2-nitrophenyl)acetamide (0.5 g, 2.33 mmol) in dimethylformamide (DMF) (5 mL) was added into the above solution quickly, and stirring was continued at 50 °C for 15 min. Then, the reaction solution was alkalized to pH 9 with aqueous Na_2CO_3. Subsequently, the mixture was filtered, and the cake was washed with H_2O and EtOAc. The combined filtrate was extracted with EtOAc. Then, the combined organic layers were washed with brine, dried over anhydrous $MgSO_4$, filtered, and concentrated under reduced pressure. Purification of the crude product by chromatography on silica gel (cyclohexane/EtOAc, 4:6) afforded *N*-(2-aminophenyl)-2-chloroacetamide (**5**) as a white solid (260 mg, 60%). ^{1}H NMR (400 MHz, $CDCl_3$) δ 8.19 (s, 1H), 7.31 (dd, J = 7.8, 1.5 Hz, 1H), 7.10 (td, J = 7.7, 1.5 Hz, 1H), 6.87−6.80 (m, 2H), 4.24 (s, 2H), 3.77 (s, 2H).

*2-Chloro-N-(2-nitrosophenyl)acetamide (**6**).* *N*-(2-Aminophenyl)-2-chloroacetamide (**5**) (250 mg, 1.35 mmol) was suspended in 5 mL of CH_2Cl_2. Oxone (630 mg, 2.05 mmol) in 20 mL of water was added, and the resulting mixture was stirred vigorously for 1 h at room temperature. The organic phase was separated, and the aqueous phase was extracted with 10 mL of CH_2Cl_2. The combined organic phases

https://doi.org/10.1021/acs.jmedchem.1c00504
J. Med. Chem. 2021, 64, 9259−9270

were washed with 1 M HCl (50 mL), saturated aqueous $NaHCO_3$ (50 mL), and water (50 mL). Finally, it was dried over $MgSO_4$ and evaporated under reduced pressure to afford the nitroso derivative (**5**), which was used in the next step without further purification.

*2-Chloro-N-(2-(pyridin-3-yldiazenyl)phenyl)acetamide (**7a**).* Compound **6** (155 mg, 0.78 mmol) and 3-aminopyridine (147 mg, 1.56 mmol) were dissolved in glacial acetic acid (30 mL) and stirred for 24 h at 60 °C. The solution was diluted with water and extracted with EtOAc. The organic phase was washed four times with water and once with brine and dried over $MgSO_4$. The crude product was purified by chromatography (eluent: cyclohexane/EtOAc, 9:1) to yield **7a** (100 mg, 47%) as an orange solid. ^{1}H NMR (400 MHz, $CDCl_3$) δ 10.96 (s, 1H), 9.23 (dd, J = 2.4, 0.8 Hz, 1H), 8.73 (dd, J = 4.7, 1.6 Hz, 1H), 8.68 (dd, J = 8.4, 1.3 Hz, 1H), 8.15 (ddd, J = 8.2, 2.4, 1.6 Hz, 1H), 7.92 (dd, J = 8.1, 1.6 Hz, 1H), 7.55 (ddd, J = 8.7, 7.2, 1.6 Hz, 1H), 7.48 (ddd, J = 8.2, 4.8, 0.8 Hz, 1H), 7.29−7.22 (m, 1H), 4.29 (s, 2H). ^{13}C NMR (101 MHz, $CDCl_3$) δ 164.33, 152.27, 147.88, 147.31, 139.79, 135.65, 133.91, 127.05, 124.63, 124.31, 120.30, 120.05, 43.58.

*2-Chloro-N-(2-(phenyldiazenyl)phenyl)acetamide (**7b**).* Compound **6** (170 mg, 0.86 mmol) and aniline (159 mg, 1.71 mmol) were dissolved in glacial acetic acid (30 mL) and stirred for 4 days at room temperature. The solution was diluted with water and extracted with EtOAc. The organic phase was washed four times with water and once with brine and dried over $MgSO_4$. The crude product was purified by chromatography (eluent: cyclohexane/EtOAc, 9:1) to yield **7b** (130 mg, 56%) as an orange solid. ^{1}H NMR (400 MHz, $CDCl_3$) δ 11.03 (s, 1H), 8.66 (dd, J = 8.3, 1.3 Hz, 1H), 7.97−7.91 (m, 2H), 7.89 (ddd, J = 8.2, 1.6, 0.5 Hz, 1H), 7.56−7.46 (m, 4H), 7.22 (ddd, J = 8.2, 7.3, 1.3 Hz, 1H), 4.27 (s, 2H). ^{13}C NMR (101 MHz, $CDCl_3$) δ 164.28, 152.51, 139.63, 135.29, 132.90, 131.66, 129.39, 124.46, 123.01, 120.08, 119.98, 43.52.

*2-Chloro-N-(2-((4-(dimethylamino)phenyl)diazenyl)phenyl)-acetamide (**7c**).* Compound **6** (500 mg, 2.52 mmol) and 4-amino-*N*,*N*-dimethylaniline (514 mg, 3.78 mmol) were dissolved in glacial acetic acid (20 mL) and stirred for 30 min at room temperature. The solution was concentrated under reduced pressure and the crude product was purified by chromatography (eluent: cyclohexane/AcOEt, 8:2) to afford **7c** as a red solid in quantitative yield. ^{1}H NMR (400 MHz, $CDCl_3$) δ 11.00 (s, 1H), 8.59 (dd, J = 8.3, 1.4 Hz, 1H), 7.94−7.87 (m, 2H), 7.83 (ddd, J = 8.1, 1.6, 0.5 Hz, 1H), 7.39 (dddd, J = 8.3, 7.3, 1.6, 0.5 Hz, 1H), 7.19 (dddd, J = 8.0, 7.3, 1.3, 0.5 Hz, 1H), 6.81−6.72 (m, 2H), 4.27 (s, 2H), 3.11 (s, 6H). ^{13}C NMR (101 MHz, $CDCl_3$) δ 164.04, 152.87, 143.71, 140.36, 134.62, 130.79, 125.35, 124.46, 119.78, 118.42, 111.73, 43.61, 40.43.

*(E)-2-(4-Methylpiperazin-1-yl)-N-(2-(pyridin-3-yldiazenyl)-phenyl)acetamide (Cryptozepine-**1**).* Compound **7a** (100 mg, 0.364 mmol) was dissolved in 20 mL of MeCN. 1-Methylpiperazine (55 mg, 0.547 mmol) and triethylamine (55.3 mg, 0.546 mmol) were then slowly added to the solution. The mixture was stirred under reflux for 3 h. Upon completion, MeCN was removed under reduced pressure and the obtained oil was dissolved in EtOAc. The resulting organic solution was washed 4 times using 30 mL of saturated aqueous $NaHCO_3$. The organic layer was dried over $MgSO_4$ and evaporated under reduced pressure to afford the final product (**1**) as a yellow solid (quantitative yield). ^{1}H NMR (400 MHz, $CDCl_3$) δ 10.97 (s, 1H), 9.25 (dd, J = 2.4, 0.8 Hz, 1H), 8.78 (dd, J = 8.4, 1.3 Hz, 1H), 8.74 (dd, J = 4.8, 1.6 Hz, 1H), 8.26 (ddd, J = 8.2, 2.4, 1.6 Hz, 1H), 7.81 (dd, J = 8.2, 1.5 Hz, 1H), 7.58−7.44 (m, 2H), 7.15 (ddd, J = 8.4, 7.3, 1.3 Hz, 1H), 3.25 (s, 2H), 2.73−2.39 (m, 8H), 2.23 (s, 3H). ^{13}C NMR (101 MHz, $CDCl_3$) δ 168.84, 151.95, 146.57, 139.99, 137.85, 134.10, 129.63, 128.23, 124.11, 123.65, 120.35, 116.24, 63.03, 55.04, 53.71, 45.95.

(E)-1-Methyl-4-(2-oxo-2-((2-(pyridin-3-yldiazenyl)phenyl)-amino)ethyl)piperazine-1,4-diium chloride (Cryptozepine-1 dihydrochloride). A total of 5 mL of 4 M HCl in dioxane were added slowly to compound **1** (10 mg, 0.03 mmol) at 0 °C. The mixture was stirred for 30 min at room temperature, then the solvent and excess of HCl were evaporated under reduced pressure, and the resulting solid was washed 3 times with Et_2O (30 mL). The so obtained orange solid was dried under vacuum to afford cryptozepine-**1** dihydrochloride (quantitative yield). ^{1}H NMR (500 MHz, D_2O) δ 9.23 (s, 1H), 8.88 (s, 1H), 8.70 (d, J = 8.4, 1.7 Hz, 1H), 8.09 (dd, J = 8.3, 5.4 Hz, 1H), 8.03 (d, J = 8.2 Hz, 1H), 7.82 (d, J = 8.2, 1.5 Hz, 1H), 7.72 (t, 1H), 7.44 (t, 1H), 3.61 (s, 2H), 3.58−3.00 (m, 8H), 2.88 (s, 3H). ^{13}C NMR (126 MHz, D_2O) δ 170.19, 149.25, 145.58, 143.06, 140.05, 135.59, 134.71, 134.43, 127.04, 126.49, 124.01, 116.79, 59.48, 52.94, 49.49, 42.71. HR-MS (ESI, $[M + H]^+$): calcd for $C_{18}H_{23}N_6O^+$, 339.19; found 339.1930.

*(E)-2-(4-Methylpiperazin-1-yl)-N-(2-(phenyldiazenyl)phenyl)-acetamide (Cryptozepine-**2**).* Compound **7b** (100 mg, 0.364 mmol) was dissolved in 20 mL of MeCN. 1-Methylpiperazine (55 mg, 0.547 mmol) and triethylamine (55.3 mg, 0.546 mmol) were then slowly added to the solution. The mixture was stirred under reflux for 3 h. Upon completion, MeCN was removed under reduced pressure and the obtained oil was dissolved in EtOAc. The resulting organic solution was washed 4 times using 30 mL of saturated aqueous $NaHCO_3$. The organic layer was dried over $MgSO_4$ and evaporated under reduced pressure to afford the final product (**2**) as a yellow solid (quantitative yield). ^{1}H NMR (400 MHz, $CDCl_3$) δ 10.94 (s, 1H), 8.77 (dd, J = 8.4, 1.3 Hz, 1H), 8.07−7.97 (m, 2H), 7.78 (dd, J = 8.2, 1.6 Hz, 1H), 7.58−7.44 (m, 4H), 7.12 (ddd, J = 8.3, 7.2, 1.3 Hz, 1H), 3.23 (s, 2H), 2.82−2.30 (m, 8H), 2.22 (s, 3H). ^{13}C NMR (101 MHz, $CDCl_3$) δ 168.74, 152.75, 139.91, 137.41, 133.04, 131.31, 129.29, 123.49, 123.29, 120.09, 116.01, 63.02, 54.92, 53.73, 45.95.

(E)-1-Methyl-4-(2-oxo-2-((2-(phenyldiazenyl)phenyl)amino)-ethyl)piperazine-1,4-diium chloride (Cryptozepine-2 dihydrochloride). A total of 6 mL of 4 M HCl in dioxane was added slowly to compound **2** (50 mg, 0.15 mmol) at 0 °C. The mixture was stirred for 30 min at room temperature, then the solvent and excess of HCl were evaporated under reduced pressure, and the resulting solid was washed 3 times with Et_2O (30 mL). The so obtained orange solid was dried under vacuum to afford cryptozepine-**2** dihydrochloride (quantitative yield). ^{1}H NMR (400 MHz, DMSO-d_6) δ 10.74 (s, 1H), 8.41 (d, J = 8.3 Hz, 1H), 8.06−7.91 (m, 2H), 7.84−7.55 (m, 5H), 7.32−7.25 (m, 1H), 3.52−2.87 (m, 10H), 2.69 (s, 3H). ^{13}C NMR (126 MHz, DMSO-d_6) δ 153.28, 152.26, 136.30, 132.77, 131.81, 129.58, 128.87, 124.48, 122.98, 120.02, 116.13, 58.52, 50.68, 48.77, 41.88. HR-MS (ESI, $[M + H]^+$): calcd for $C_{19}H_{24}N_5O^+$, 338.20; found 338.1968.

*(E)-N-(2-((4-(Dimethylamino)phenyl)diazenyl)phenyl)-2-(4-methylpiperazin-1-yl)acetamide (Cryptozepine-**3**).* Compound **7c** (20 mg, 0.063 mmol) was dissolved in 20 mL of MeCN. 1-Methylpiperazine (9.5 mg, 0.095 mmol) and triethylamine (9.58 mg, 0.095 mmol) were then slowly added to the solution. The mixture was stirred under reflux for 3 h. Upon completion, MeCN was removed under reduced pressure and the obtained oil was dissolved in EtOAc. The resulting organic solution was washed 4 times using 30 mL of saturated aqueous $NaHCO_3$. The organic layer was dried over $MgSO_4$ and evaporated under reduced pressure to afford the final product (**3**) as a yellow solid (quantitative yield). ^{1}H NMR (400 MHz, $CDCl_3$) δ 10.90 (s, 1H), 8.72 (dd, J = 8.4, 1.3 Hz, 1H), 8.03−7.98 (m, 2H), 7.75 (dd, J = 8.1, 1.6 Hz, 1H), 7.38 (ddd, J = 8.6, 7.3, 1.6 Hz, 1H), 7.11 (ddd, J = 8.3, 7.3, 1.4 Hz, 1H), 6.82−6.74 (m, 2H), 3.24 (s, 2H), 3.11 (s, 6H), 2.83−2.43 (m, 8H), 2.29 (s, 3H). ^{13}C NMR (101 MHz, $CDCl_3$) δ 168.61, 152.65, 143.93, 140.49, 136.28, 131.02, 125.61, 123.56, 119.80, 115.65, 111.67, 63.13, 54.97, 53.78, 45.98, 40.43.

(E)-1-(2-((2-((4-(Dimethylamino)phenyl)diazenyl)phenyl)amino)-2-oxoethyl)-4-methylpiperazine-1,4-diium (Cryptozepine-3 dihydrochloride). A total of 6 mL of 4 M HCl in dioxane was added slowly to compound **3** (10 mg, 0.026 mmol) at 0 °C. The mixture was stirred for 30 min at room temperature, then the solvent and excess of HCl were evaporated under reduced pressure, and the resulting solid was washed 3 times with Et_2O (30 mL). The so obtained orange solid was dried under vacuum to afford cryptozepine-**3** dihydrochloride (quantitative yield). ^{1}H NMR (400 MHz, D_2O) δ 8.01 (d, J = 8.2 Hz, 1H), 7.91−7.77 (m, 2H), 7.65−7.53 (m, 2H), 7.36 (d, 3H), 3.82−2.61 (m, 19H). ^{13}C NMR (101 MHz, D_2O) δ ^{13}C NMR (101 MHz, D_2O) δ 168.82, 149.08, 147.06, 141.60, 133.70, 131.88, 125.79,

https://doi.org/10.1021/acs.jmedchem.1c00504
J. Med. Chem. 2021, 64, 9259−9270

125.00, 122.23, 116.67, 116.55, 59.48, 52.67, 49.44, 42.72, 42.67. HR-MS (ESI, $[M + H]^+$): calcd for $C_{21}H_{29}N_6O^+$, 381.24; found 381.2387.

*2-Fluoro-4-nitro-1-nitrosobenzene (**8**).* 2-Fluoro-4-nitroaniline (500 mg, 3.20 mmol) was suspended in 10 mL of CH_2Cl_2. Oxone (2.46 g, 8.00 mmol) in 20 mL of water was then added, and the resulting mixture was stirred vigorously for 24 h at room temperature. The organic phase was separated, and the aqueous phase was further extracted with 10 mL of CH_2Cl_2 3 times. The combined organic phases were washed with 1 M HCl (50 mL), saturated aqueous $NaHCO_3$ (50 mL), and water (50 mL). Finally, it was dried over $MgSO_4$, concentrated under reduced pressure, and purified by chromatography (eluent: cyclohexane/EtOAc, 9:1) to yield **8** as a green solid (300 mg, 55%), which was immediately used in the following step without further purification.

*2-Chloro-N-(2-((2-fluoro-4-nitrophenyl)diazenyl)phenyl)-acetamide (**9**).* Compounds **5** (500 mg, 2.71 mmol) and **8** (250 mg, 1.47 mmol) were dissolved in glacial acetic acid (20 mL), and the resulting solution was stirred for 24 h at room temperature. The solution was then concentrated under reduced pressure, and the crude material was purified by chromatography (eluent: cyclohexane/EtOAc, 9:1). The so obtained solid was further purified by crystallization from methanol to yield **9** as an orange solid (200 mg, 40%). ^{1}H NMR (400 MHz, $CDCl_3$) δ 10.83 (s, 1H), 8.70 (dd, J = 8.5, 1.3 Hz, 1H), 8.33−8.08 (m, 2H), 7.95 (dd, J = 8.2, 1.6 Hz, 1H), 7.90−7.84 (m, 1H), 7.61 (ddd, J = 8.7, 7.4, 1.6 Hz, 1H), 7.30−7.24 (m, 1H), 4.29 (s, 2H). ^{13}C NMR (101 MHz, $CDCl_3$) δ 164.35, 144.45, 140.28, 136.53, 135.36, 126.98, 124.83, 124.75, 120.49, 120.07, 119.85, 119.81, 119.23, 43.56.

*(E)-N-(2-((2-Fluoro-4-nitrophenyl)diazenyl)phenyl)-2-(4-methyl-piperazin-1-yl)acetamide (Cryptozepine-**4**).* Compound **9** (200 mg, 0.594 mmol) was dissolved in 20 mL of MeCN. 1-Methylpiperazine (89.24 mg, 0.891 mmol) and triethylamine (90.16 mg, 0.891 mmol) were then slowly added to the solution. The mixture was stirred under reflux for 3 h. Upon completion, MeCN was removed under reduced pressure and the obtained oil was dissolved in EtOAc. The resulting organic solution was washed 4 times using 30 mL of saturated aqueous $NaHCO_3$. The organic layer was dried over $MgSO_4$ and evaporated under reduced pressure to afford the desired final compound (**4**) as an orange solid (quantitative yield). ^{1}H NMR (400 MHz, $CDCl_3$) δ 10.94 (s, 1H), 8.80 (dd, J = 8.5, 1.3 Hz, 1H), 8.27−8.11 (m, 2H), 8.04−7.93 (m, 1H), 7.85 (dd, J = 8.3, 1.6 Hz, 1H), 7.58 (ddd, J = 8.6, 7.2, 1.6 Hz, 1H), 7.16 (ddd, J = 8.4, 7.2, 1.3 Hz, 1H), 3.26 (s, 2H), 2.80−2.30 (m, 8H), 2.21 (s, 3H). ^{13}C NMR (101 MHz, $CDCl_3$) δ 168.86, 160.09, 157.48, 140.43, 138.63, 135.52, 123.79, 120.55, 119.88, 119.43, 116.84, 113.78, 113.53, 62.93, 55.17, 53.63, 46.07. HR-MS (ESI, $[M + H]^+$): calcd for $C_{19}H_{22}FN_6O_3^+$, 401.17; found 401.1732.

***In Vitro* Radioligand Competition Binding Experiments.** The affinity of our compounds and pirenzepine (PNZ) for mAChRs was studied by radioligand competition binding experiments (see Table 1 and Figure S5.1). The Wistar rat brain membranes (whole cortex), which contain a high density of mAChRs, were used for this assay.[28] The muscarinic antagonist [^{3}H]quinuclidinyl benzilate ([^{3}H]QNB) in ethanol solution from Amersham Biosciences (catalog number TRK 604, 42 Ci/mmol, 1 mCi/mL) was used as a competitive radioligand.[30,41] Specific binding was defined with the new ligands at total nominal concentrations ranging from 1 or 10 nM to 300 μM, and derivatizing the raw disintegrations per minute (dpm) data from the scintillation counter to show the total radioactivity.[28] Binding assays were carried out as already reported by Claro.[28] Brain membranes were prepared from 2−3-month-old female rats. The meninges were cleaned with buffer-soaked filter paper, cortices were dissected, and white matter was trimmed off. The tissues were homogenized in 40 mL of Tris−HCl buffer using a Potter homogenizer with a motor-driven Teflon pestle. The homogenate was centrifuged (30 min at 50 000g). The resulting pellet was homogenized and centrifuged again under the same conditions. The Bradford assay was used for protein determination. The final pellet was resuspended at 1 mg protein/mL, transferred to 1 mL microcentrifuge tubes, and centrifuged again. After discarding the supernatant, membrane pellets were kept at −80 °C until use. During the assay, in 5 mL tubes (24 tubes in each experiment repetition), a total volume of 2 mL of Tris−HCl buffer with 6 mM $MgCl_2$ was used, containing 30 μg of mAChR proteins, 200 pM [^{3}H]QNB concentration ([^{3}H]QNB K_d = 40 pM), and the correct amount of our ligands. These conditions ensure less than 10% ligand depletion at equilibrium, which was reached with 30 min at 37 °C incubation. The unbound ligand and radioligand were separated from the membrane samples by rapid filtration through Whatman GF/C glass microfiber filters using a manyfold Brandel device. Nonspecific binding was independent of protein concentration and defined with 2 μM atropine. It resulted to be lower than 5% of total binding.

***In Vitro* Calcium Imaging Experiments.** *Cell Culture and Transfection for Calcium Imaging.* TsA201 cells were purchased from the European Collection of Authenticated Cell Culture. The cells were maintained at 37 °C in a humidified atmosphere with 5% CO_2 and grown in Dulbecco's modified Eagle's medium/Nutrient Mixture F-12 Ham (DMEM/F12 1:1, Life Technologies) medium, supplemented with 10% fetal bovine serum (FBS, Life Technologies) and antibiotics (1% penicillin/streptomycin, Sigma-Aldrich). The cells were transiently transfected with the human M_1 receptor (Addgene), cotransfected with M_1 and R-GECO1 (ratio: 1:1), or human M_2 receptor (Addgene), and chimeric Gi/Gq protein (GqTOP) (ratio: 1:1), using X-tremeGENE 9 DNA Transfection Reagent (Roche Applied Science) following the manufacturer's instructions. As generally known, M_1 mAChRs prevalently activate Gq proteins and lead to the activation of the phospholipase C pathway, resulting in the production of inositol 1,4,5-trisphosphate (IP3) and the subsequent release of intracellular calcium from the endoplasmic reticulum. In contrast, the M_2 mAChR prevalently activates the Gi protein; therefore, we cotransfected the cells with a chimeric Gq/i-protein, which couples M_2 activation with the phospholipase C pathway. After 24 h, the cells were harvested with Accutase (Sigma-Aldrich) and plated onto 16 mm glass coverslips (Fisher Scientific) pretreated with poly-L-lysine (Sigma-Aldrich) to allow cell adhesion. Preconfluent cultures were used for experiments between 48 and 72 h after transfection.

In Vitro Single-Cell Calcium Imaging. The bath solution used for single-cell intracellular calcium recordings contained 140 mM NaCl, 5.4 mM KCl, 1 mM $MgCl_2$, 10 mM HEPES, 10 mM glucose, and 2 mM $CaCl_2$ (pH 7.4). The calcium indicator used to test cryptozepine-**2** was OGB-1 AM (Life Technologies). Before each experiment, the cells were mounted on the recording chamber (Open Diamond Bath Imaging Chamber for Round Coverslips from Warner Instruments) and loaded with OGB-1 AM for 30 min at 37 °C with 5% CO_2 at a final concentration of 10 μM in Ca^{2+}-free bath solution. The cells were rinsed with fresh solution, and the recording chamber was filled with 1 mL of recording solution and placed on an IX71 inverted microscope (Olympus) with an XLUMPLFLN 20XW x20/1 water immersion objective (Olympus). OGB-1 AM was excited during 50 ms at 488 nm using a Polychrome V light source (Till Photonics) equipped with a Xenon Short-Arc lamp (Ushio) and a 505 nm dichroic beam splitter (Chroma Technology). The emission at 510 nm was filtered by a D535/40 nm emission filter (Chroma Technology) and finally collected by a C9100-13 EM-CCD camera (HAMAMATSU). R-GECO1 was used as a Ca^{2+} fluorescent indicator because it absorbs less than OGB-1-AM at 460 nm, a wavelength used to photoisomerize the compound cryptozepine-**3**. R-GECO1 was excited during 50 ms at 562 nm using a Polychrome V light source (Till Photonics) equipped with a Xenon Short-Arc lamp (Ushio) and a 585 nm dichroic beam splitter (Chroma Technology). The emission at 600 nm was filtered using an ET630/75 nm emission filter (Chroma Technology) and finally collected by a C9100-13 EM-CCD camera (HAMAMATSU). Images were acquired at room temperature with an imaging interval of 2 s with SmartLux software (HEKA), and the imaging analysis was performed with FIJI (ImageJ). The agonist used to stimulate M_1 and M_2 receptors in HEK tsA201 cells was acetylcholine (ACh, Sigma). The application of the compounds was carried out by manually pipetting a small volume during imaging acquisition into the accessory pool of the recording

https://doi.org/10.1021/acs.jmedchem.1c00504
J. Med. Chem. 2021, 64, 9259−9270

chamber for the final dilution of approximately 1:1000. Every application of 0.5 ACh μM was followed by the next application after a 20-min recovery time. The effect of these photoswitchable antagonists on the ACh-induced calcium signal was observed by applying each compound (100 μM) for 2 min in its *trans* or *cis* form prior to the ACh application. The subtype-selectivity study (M_1 vs M_2 mAChRs) of cryptozepine-**2** was performed by comparing the amplitude of calcium signal response of cells expressing M_2-GqTOP or M_1 mAChR in the presence of different concentrations of cryptozepine-**2** (10, 30, 50, and 100 μM). Data were normalized over the maximum response obtained with ACh at 0.5 μM. In the case of pirenzepine, it was applied at decreasing concentrations ranging from 10 nM to 100 μM, 2 min before ACh. Photoisomerization of cryptozepine-**2** was achieved by preilluminating the compounds with a Vilber Lourmat UV Lamp (365 nm, 6 W) for 2 min before application. Photoisomerization of cryptozepine-**3** was achieved by continuously illuminating the specimen with 460 nm light. Numerical data were imported to GraphPad Prism version 6.00 for Windows (GraphPad Software, La Jolla, CA). Statistical analysis was performed using the paired-sample Wilcoxon signed-rank test.

***In Vitro* Specific M_1 and M_2 Muscarinic Binding Assay Study of *cis*-Cryptozepine-2.** The *in vitro* radioligand binding assay of 1, 10, and 100 μM *cis*-cryptozepine-**2** enriched form (active isomer) was assessed on recombinant human M_1 and M_2 receptors expressed in Chinese hamster ovary (CHO) cells. A 10 mM DMSO stock solution of the compound was used for the assay after 30 min irradiation with 365 nm light to work with a high percentage of the active *cis* isomer (>80%). The compound affinity was calculated as a percentage inhibition of the binding of a radioactively labeled antagonist specific for each target to assess the subtype-specific binding of cryptozepine-**2**. In particular, 2 nM [^{3}H]-pirenzepine for M_1 and 2 nM [^{3}H]AF-DX 384 for M_2 were used as subtype-selective radioligand. The evaluation of the affinity of cryptozepine-**2** for the human M_1 receptor was carried out using cell membrane homogenates (45 μg of protein) incubated for 60 min at 22 °C with 2 nM [^{3}H]pirenzepine (K_d = 13 nM) in the absence or presence of the test compound in a buffer containing 50 mM Tris−HCl (pH 7.4), 120 mM NaCl, 5 mM KCl, 5 mM $MgCl_2$, and 1 mM EDTA. Nonspecific binding was determined in the presence of 1 μM atropine. Following incubation, the samples were filtered rapidly under vacuum through glass fiber filters (GF/B, Packard) presoaked with 0.3% PEI and rinsed several times with ice-cold 50 mM Tris−HCl using a 96-sample cell harvester (Unifilter, Packard). The filters are dried and then counted for radioactivity in a scintillation counter (Topcount, Packard) using a scintillation cocktail (MicroScint 0, Packard). The standard reference compound was pirenzepine, which was tested in each experiment at several concentrations to obtain a competition curve from which its IC_{50} is calculated.[42]

For evaluating the affinity of cryptozepine-**2** for the human M_2 receptor, cell membrane homogenates (60 μg protein) were incubated with 2 nM [3H]AF-DX 384 (K_d = 4.6 nM) following the same procedure described for the M_1 receptors. The standard reference compound was methoctramine, which was tested in each experiment at several concentrations to obtain a competition curve from which its IC_{50} is calculated.[42] The results showing an inhibition higher than 50% are considered to represent significant effects of the test compounds. The results showing an inhibition between 25 and 50% are indicative of weak to moderate effects. The results showing an inhibition lower than 25% are not considered significant. Experiments were performed in duplicate and accepted in accordance with Eurofins Cerep Quality Control Unit's validation standard operating procedure.

***Ex Vivo* Mice Atria Tissue Experiments.** *Animals and Tissue Samples.* Ten CD1 male mice of 10−12 weeks old were used. Housing was under controlled conditions: constant temperature (22 ± 2 °C) and humidity (55 ± 10%), a 12-h light/dark cycle, and ad libitum access to water and food. Before euthanasia, heparin (100 units/kg IP) was administered. Animals were sacrificed by cervical dislocation under sedation with ketamine (80 mg/kg IP) and xylazine (10 mg/kg IP). For functional studies, heart was quickly removed and placed in carbogenated (95% O_2 and 5% CO_2) Krebs solution (composition in mmol/L: glucose 10.10, NaCl 115.48, $NaHCO_3$ 21.90, KCl 4.61, NaH_2PO_4 1.14, $CaCl_2$ 2.50, and $MgSO_4$ 1.16) (pH 7.4). Functional experiments were approved by the Ethics Committee of the Universitat Autònoma de Barcelona (code EUT-MJ001).

Functional Studies. Right atrium was isolated and mounted in a 10 mL chamber using a compact organ bath (Panlab SL). The tissue was bathed in a carbogenated Krebs solution maintained at 37 ± 1 °C using an external thermostat. The mechanical activity was measured with an isometric force transducer connected to a computer through an amplifier associated with PowerLab/800. LabChart software was used for data digitalization (1000 samples/s) and measurements. A tension of 0.2 g was applied, and the tissue was allowed to equilibrate for 5−10 min until spontaneous mechanical contractions were recorded. Carbachol (10^{-6} M) was added for 3 min and then 10^{-6} and 10^{-5} M pirenzepine (PNZ), 10^{-5}, 3×10^{-5}, and 10^{-4} M *trans*-cryptozepine-**2** (*trans*), or 10^{-5}, 3×10^{-5}, and 10^{-4} M *cis*-cryptozepine-**2** (*cis*) were applied. Amplitude and beats per minute (beats/min, bpm) were calculated before and after the addition of the drug. Atrial contractions were recorded at a frequency of about 360 beats/min and a mean amplitude of 0.1 g. Carbachol (CCh) concentration-dependently decreased both the amplitude and beats/min (n = 6) with an EC50 of about 10^{-6} M. This concentration of CCh was used to activate muscarinic receptors in the bioassay and induces bradycardia. The presence of both pirenzepine (PNZ) (n = 6) and *cis*-cryptozepine-**2** (*cis*) (n = 2) concentration-dependently reversed the effect of 10^{-6} M CCh in terms of heartbeat frequency. In contrast, *trans*-cryptozepine-**2** (*trans*) (n = 2) did not reserve CCh-induced bradycardia (n = 2) (Figures 4, S7.1, and S7.2).

■ ASSOCIATED CONTENT

Supporting Information

The Supporting Information is available free of charge at https://pubs.acs.org/doi/10.1021/acs.jmedchem.1c00504.

Molecular docking simulations; HPLC analyses and mass spectra; photochemical characterization; NMR spectroscopy; *in vitro* radioligand competition binding experiments; *in vitro* calcium imaging experiments; *ex vivo* mice atria tissue experiments (PDF)

Molecular formula strings (CSV)

■ AUTHOR INFORMATION

Corresponding Author

Pau Gorostiza − *Institute for Bioengineering of Catalonia (IBEC), Barcelona Institute for Science and Technology (BIST), Barcelona 08028, Spain; Network Biomedical Research Center in Bioengineering, Biomaterials, and Nanomedicine (CIBER-BBN), Madrid 28029, Spain; Catalan Institution for Research and Advanced Studies (ICREA), Barcelona 08010, Spain;* orcid.org/0000-0002-7268-5577; Email: pau@icrea.cat

Authors

Fabio Riefolo − *Institute for Bioengineering of Catalonia (IBEC), Barcelona Institute for Science and Technology (BIST), Barcelona 08028, Spain; Network Biomedical Research Center in Bioengineering, Biomaterials, and Nanomedicine (CIBER-BBN), Madrid 28029, Spain;* Present Address: Teamit Research, Barcelona Health Hub, Barcelona 08025, Spain.; orcid.org/0000-0002-6762-2619

Rosalba Sortino − *Institute for Bioengineering of Catalonia (IBEC), Barcelona Institute for Science and Technology (BIST), Barcelona 08028, Spain; Network Biomedical*

Research Center in Bioengineering, Biomaterials, and Nanomedicine (CIBER-BBN), Madrid 28029, Spain

Carlo Matera − *Institute for Bioengineering of Catalonia (IBEC), Barcelona Institute for Science and Technology (BIST), Barcelona 08028, Spain; Network Biomedical Research Center in Bioengineering, Biomaterials, and Nanomedicine (CIBER-BBN), Madrid 28029, Spain; Department of Pharmaceutical Sciences, University of Milan, Milan 20133, Italy;* orcid.org/0000-0001-6939-3859

Enrique Claro − *Institut de Neurociències and Departament de Bioquímica i Biologia Molecular, Unitat de Bioquímica de Medicina, Universitat Autònoma de Barcelona (UAB), Barcelona 08193, Spain*

Beatrice Preda − *Institute for Bioengineering of Catalonia (IBEC), Barcelona Institute for Science and Technology (BIST), Barcelona 08028, Spain*

Simone Vitiello − *Institute for Bioengineering of Catalonia (IBEC), Barcelona Institute for Science and Technology (BIST), Barcelona 08028, Spain;* Present Address: Department of Life Sciences, University of Modena and Reggio Emilia, Via Campi 103, 41125 Modena, Italy.

Sara Traserra − *Department of Cell Biology, Physiology and Immunology, Universitat Autonoma de Barcelona, Barcelona 08193, Spain*

Marcel Jiménez − *Department of Cell Biology, Physiology and Immunology, Universitat Autonoma de Barcelona, Barcelona 08193, Spain; Centro de Investigación Biomédica en Red de Enfermedades Hepáticas y Digestivas (CIBERehd), Instituto de Salud Carlos III, Madrid 28029, Spain*

Complete contact information is available at: https://pubs.acs.org/10.1021/acs.jmedchem.1c00504

Author Contributions

¶R.S. and C.M. contributed equally to this work. This manuscript was written through contributions of all authors. All authors have given approval to the final version of the manuscript.

Funding

This project has received funding from European Union Research and Innovation Programme Horizon 2020 (Human Brain Project SGA2 Grant Agreement 785907 and SGA3 No. 945539), DEEPER (Grant No. 101016787), ERASynBio programme (Modulightor project funded by Ministry of Economy and Competitiveness, Grant No. PCIN-2015-163-C02-02), and financial support from Generalitat de Catalunya through the Agency for Management of University and Research Grants (Grant No. 2017-SGR-1442), the General Directorate for Research (Grant No. IU16- 011593, co-funded with FEDER Operational Program of Catalonia 2014−2020) and CERCA Programme; Ministry of Science and Innovation/FEDER (Grants CTQ2016-80066-R, PID2019-111493RB-I00, SAF2017-88019-C3-1-R), and "La Caixa" Foundation (Grant No. LCF/PR/HR19/52160010).

Notes

The authors declare no competing financial interest.

■ ACKNOWLEDGMENTS

The authors are grateful to Jean-Philippe Pin for providing the chimeric Gi/Gq protein clone. Molecular graphics and analyses were performed with the UCSF Chimera package. Chimera is developed by the Resource for Biocomputing, Visualization, and Informatics at the University of California, San Francisco (supported by NIGMS P41-GM103311). Mass spectrometry was performed at the IRB Barcelona Mass Spectrometry Core Facility, which actively participates in the BMBS European COST Action BM 1403 and is a member of Proteored, PRB2-ISCIII, supported by grant PRB2 (IPT13/0001—ISCIIISGE-FI/FEDER). The authors thank Dr. Unai Elezcano and Dr. Sònia Varón from the Analysis and Chemistry Platform (PQA-PCB) at Barcelona Science Park for their help in HPLC-MS experiments throughout the project. All animal procedures were experiments approved by the Ethics Committee of the Universitat Autònoma de Barcelona (code EUT-MJ001).

■ REFERENCES

(1) Lerch, M. M.; Hansen, M. J.; van Dam, G. M.; Szymanski, W.; Feringa, B. L. Emerging Targets in Photopharmacology. *Angew. Chem., Int. Ed.* **2016**, *55*, 10978−10999.

(2) Hüll, K.; Morstein, J.; Trauner, D. In Vivo Photopharmacology. *Chem. Rev.* **2018**, 10710−10747.

(3) Morstein, J.; Awale, M.; Reymond, J. L.; Trauner, D. Mapping the Azolog Space Enables the Optical Control of New Biological Targets. *ACS Cent. Sci.* **2019**, *5*, 607−618.

(4) Pittolo, S.; Gómez-Santacana, X.; Eckelt, K.; Rovira, X.; Dalton, J.; Goudet, C.; Pin, J. P.; Llobet, A.; Giraldo, J.; Llebaria, A.; Gorostiza, P. An Allosteric Modulator to Control Endogenous G Protein-Coupled Receptors with Light. *Nat. Chem. Biol.* **2014**, *10*, 813−815.

(5) Schoenberger, M.; Damijonaitis, A.; Zhang, Z.; Nagel, D.; Trauner, D. Development of a New Photochromic Ion Channel Blocker via Azologization of Fomocaine. *ACS Chem. Neurosci.* **2014**, *5*, 514−518.

(6) Matera, C.; Gomila, A. M. J.; Camarero, N.; Libergoli, M.; Soler, C.; Gorostiza, P. Photoswitchable Antimetabolite for Targeted Photoactivated Chemotherapy. *J. Am. Chem. Soc.* **2018**, *140*, 15764−15773.

(7) Agnetta, L.; Decker, M. Photoresponsive Hybrid Compounds. In *Design of Hybrid Molecules for Drug Development*; Elsevier Inc., 2017; pp 279−315.

(8) Yet, L. *Privileged Structures in Drug Discovery*; John Wiley & Sons, Inc.: Hoboken, NJ, 2018.

(9) Evans, B. E.; Rittle, K. E.; Bock, M. G.; DiPardo, R. M.; Freidinger, R. M.; Whitter, W. L.; Lundell, G. F.; Veber, D. F.; Anderson, P. S.; Chang, R. S. L.; Lotti, V. J.; Cerino, D. J.; Chen, T. B.; Kling, P. J.; Kunkel, K. A.; Springer, J. P.; Hirshfield, J. Methods for Drug Discovery: Development of Potent, Selective, Orally Effective Cholecystokinin Antagonistsis. *J. Med. Chem.* **1988**, *31*, 2235−2246.

(10) Marsh, W. Tricyclic Antidepressants. In *xPharm: The Comprehensive Pharmacology Reference*; Elsevier Inc., 2007; pp 1−3.

(11) Fedi, V.; Guidi, A.; Altamura, M. Tricyclic Structures in Medicinal Chemistry: An Overview of Their Recent Uses in Non-CNS Pathologies. *Mini-Rev. Med. Chem.* **2008**, *8*, 1464−1484.

(12) Matera, C.; Tata, A. Pharmacological Approaches to Targeting Muscarinic Acetylcholine Receptors. *Recent Pat. CNS Drug Discovery* **2014**, *9*, 85−100.

(13) Kruse, A. C.; Kobilka, B. K.; Gautam, D.; Sexton, P. M.; Christopoulos, A.; Wess, J. Muscarinic Acetylcholine Receptors: Novel Opportunities for Drug Development. *Nat. Rev. Drug Discovery* **2014**, *13*, 549−560.

(14) Riefolo, F.; Matera, C.; Garrido-Charles, A.; Gomila, A. M. J.; Sortino, R.; Agnetta, L.; Claro, E.; Masgrau, R.; Holzgrabe, U.; Batlle, M.; Decker, M.; Guasch, E.; Gorostiza, P. Optical Control of Cardiac Function with a Photoswitchable Muscarinic Agonist. *J. Am. Chem. Soc.* **2019**, *141*, 7628−7636.

(15) Agnetta, L.; Kauk, M.; Canizal, M. C. A.; Messerer, R.; Holzgrabe, U.; Hoffmann, C.; Decker, M. A Photoswitchable Dualsteric Ligand Controlling Receptor Efficacy. *Angew. Chem., Int. Ed.* **2017**, *56*, 7282−7287.

(16) Agnetta, L.; Bermudez, M.; Riefolo, F.; Matera, C.; Claro, E.; Messerer, R.; Littmann, T.; Wolber, G.; Holzgrabe, U.; Decker, M. Fluorination of Photoswitchable Muscarinic Agonists Tunes Receptor Pharmacology and Photochromic Properties. *J. Med. Chem.* **2019**, *62*, 3009−3020.
(17) Hammer, R.; Berrie, C. P.; Birdsall, N. J. M.; Burgen, A. S. V.; Hulme, E. C. Pirenzepine Distinguishes between Different Subclasses of Muscarinic Receptors [28]. *Nature* **1980**, *283*, 90−92.
(18) El-Obeild, H. A.; Babhair, S. A.; Al-Badr, A. A. Pirenzepine Dihydrochloride. *Anal. Profiles Drug Subst. Excipients* **1987**, *16*, 445−506.
(19) Eberlein, W. G.; Engel, W. W.; Trummlitz, G.; Schmidt, G.; Hammer, R. Tricyclic Compounds as Selective Antimuscarinics. 2. Structure-Activity Relationships of M1 Selective Antimuscarinics Related to Pirenzepine. *J. Med. Chem.* **1988**, *31*, 1169−1174.
(20) Stolerman, I. P. Encyclopedia of Psychopharmacology. Springer. https://www.springer.com/gp/book/9783540687061#aboutAuthors (accessed April 3, 2020).
(21) Walline, J. J.; Lindsley, K.; Vedula, S. S.; Cotter, S. A.; Mutti, D. O.; Twelker, J. D. Interventions to Slow Progression of Myopia in Children. *Cochrane Database Syst. Rev.* **2011**, No. CD004916.
(22) Pedretti, R. F. E.; Prete, G.; Foreman, R. D.; Adamson, P. B.; Vanoli, E. Autonomic Modulation during Acute Myocardial Ischemia by Low-Dose Pirenzepine in Conscious Dogs with a Healed Myocardial Infarction: A Comparison with β-Adrenergic Blockade. *J. Cardiovasc. Pharmacol.* **2003**, *41*, 671−677.
(23) Thal, D. M.; Sun, B.; Feng, D.; Nawaratne, V.; Leach, K.; Felder, C. C.; Bures, M. G.; Evans, D. A.; Weis, W. I.; Bachhawat, P.; Kobilka, T. S.; Sexton, P. M.; Kobilka, B. K.; Christopoulos, A. Crystal Structures of the M1 and M4 Muscarinic Acetylcholine Receptors. *Nature* **2016**, *531*, 335−340.
(24) Murgolo, N. J.; Kozlowski, J.; Tice, M. A. B.; Hollinger, F. P.; Brown, J. E.; Zhou, G.; Taylor, L. A.; McQuade, R. D. The N4 Nitrogen of Pirenzepine Is Responsible for Selective Binding of the M1 Subtype Human Muscarinic Receptor. *Bioorg. Med. Chem. Lett.* **1996**, *6*, 785−788.
(25) Dong, M.; Babalhavaeji, A.; Samanta, S.; Beharry, A. A.; Woolley, G. A. Red-Shifting Azobenzene Photoswitches for in Vivo Use. *Acc. Chem. Res.* **2015**, *48*, 2662−2670.
(26) Ghetti, F.; Griesbeck, A. G.; Oelgemöller, M. *CRC Handbook of Organic Photochemistry and Photobiology*; CRC Press, 2012.
(27) Bandara, H. M. D.; Burdette, S. C. Photoisomerization in Different Classes of Azobenzene. *Chem. Soc. Rev.* **2012**, *41*, 1809−1825.
(28) Claro, E. Analyzing Ligand Depletion in a Saturation Equilibrium Binding Experiment. *Biochem. Mol. Biol. Educ.* **2006**, *34*, 428−431.
(29) Yamamura, H. I.; Snyder, S. H. Muscarinic Cholinergic Binding in Rat Brain. *Proc. Natl. Acad. Sci. U.S.A.* **1974**, *71*, 1725−1729.
(30) Sallés, J.; Wallace, M. A.; Fain, J. N. Differential Effects of Alkylating Agents on the Multiple Muscarinic Receptor Subtypes Linked to Activation of Phospholipase C by Carbachol in Rat Brain Cortical Membranes. *J. Pharmacol. Exp. Ther.* **1993**, *264*, 521−529.
(31) Massoulié, J.; Carson, S.; Kato, G. Biochemical Characterization of Muscarinic Receptors: Multiplicity of Binding Components. *Prog. Brain Res.* **1979**, *49*, 303−311.
(32) Heijman, J.; Kirchner, D.; Kunze, F.; Chrétien, E. M.; Michel-Reher, M. B.; Voigt, N.; Knaut, M.; Michel, M. C.; Ravens, U.; Dobrev, D. Muscarinic Type-1 Receptors Contribute to IK,ACh in Human Atrial Cardiomyocytes and Are Upregulated in Patients with Chronic Atrial Fibrillation. *Int. J. Cardiol.* **2018**, *255*, 61−68.
(33) Süsskand, K.; Sewing, K.-F. Anticholinergic Effects of Pirenzepine on the Guinea-Pig Isolated Atrium. *Pharmacology* **1979**, *19*, 163−164.
(34) Woo, S. H.; Byung, H. L.; Kwon, K. Il.; Chin, O. L. Excitatory Effect of M1 Muscarinic Acetylcholine Receptor on Automaticity of Mouse Heart. *Arch. Pharmacal Res.* **2005**, *28*, 930−935.
(35) Hogan, K.; Markos, F. Muscarinic Type 1 Receptors Mediate Part of Nitric Oxide's Vagal Facilitatory Effect in the Isolated Innervated Rat Right Atrium. *Nitric Oxide* **2007**, *16*, 110−117.
(36) Cabré, G.; Garrido-Charles, A.; Moreno, M.; Bosch, M.; Porta-de-la-Riva, M.; Krieg, M.; Gascón-Moya, M.; Camarero, N.; Gelabert, R.; Lluch, J. M.; Busqué, F.; Hernando, J.; Gorostiza, P.; Alibés, R. Rationally Designed Azobenzene Photoswitches for Efficient Two-Photon Neuronal Excitation. *Nat. Commun.* **2019**, *10*, No. 907.
(37) Araujo, D. M.; Lapchak, P. A.; Regenold, W.; Quirion, R. Characterization of [3H]AF-DX 116 Binding Sites in the Rat Brain: Evidence for Heterogeneity of Muscarinic-M2 Receptor Sites. *Synapse* **1989**, *4*, 106−114.
(38) Giachetti, A.; Micheletti, R.; Montagna, E. Cardioselective Profile of AF-DX 116, a Muscarine M2 Receptor Antagonist. *Life Sci.* **1986**, *38*, 1663−1672.
(39) Shrestha, R.; Mohammed, S. K.; Hasan, M. M.; Zhang, X.; Wahid, K. A. Automated Adaptive Brightness in Wireless Capsule Endoscopy Using Image Segmentation and Sigmoid Function. *IEEE Trans. Biomed. Circuits Syst.* **2016**, *10*, 884−892.
(40) Feiner, R.; Engel, L.; Fleischer, S.; Malki, M.; Gal, I.; Shapira, A.; Shacham-Diamand, Y.; Dvir, T. Engineered Hybrid Cardiac Patches with Multifunctional Electronics for Online Monitoring and Regulation of Tissue Function. *Nat. Mater.* **2016**, *15*, 679−685.
(41) Yamamura, H. I.; Snyder, S. H. Muscarinic Cholinergic Binding in Rat Brain. *Proc. Natl. Acad. Sci. U.S.A.* **1974**, *71*, 1725−1729.
(42) Dörje, F.; Wess, J.; Lambrecht, G.; Tacke, R.; Mutschler, E.; Brann, M. R. Antagonist Binding Profiles of Five Cloned Human Muscarinic Receptor Subtypes. *J. Pharmacol. Exp. Ther.* **1991**, *256*, 727−733.

https://doi.org/10.1021/acs.jmedchem.1c00504
J. Med. Chem. 2021, 64, 9259−9270